Applied Mathematical Modelling 59 (2018) 527–545

Contents lists available at ScienceDirect

Applied Mathematical Modelling

journal homepage: www.elsevier.com/locate/apm

Analysis of the damping characteristics of two power electronics-based devices using 'individual channel analysis and design'

Carlos E. Ugalde-Loo[a,*], Enrique Acha[b], Eduardo Licéaga-Castro[c]

[a] School of Engineering, Cardiff University, Queen's Buildings, The Parade, Cardiff CF24 3AA, Wales, U.K.
[b] Electrical Energy Engineering Unit, Tampere University of Technology, Korkeakoulunkatu 10, FI-33720 Tampere, Finland
[c] CIIIA-FIME, Universidad Autónoma de Nuevo León, Monterrey, Km 2.3 Carr. a Salinas Victoria, C.P. 66600 Apodaca, Nuevo León, México

ARTICLE INFO

Article history:
Received 9 August 2017
Revised 9 February 2018
Accepted 13 February 2018
Available online 20 February 2018

Keywords:
Flexible AC transmission systems
Frequency domain analysis
Individual channel analysis and design
Multivariable control
Static VAr compensator
Thyristor-controlled series compensator

ABSTRACT

A comparison of the capabilities of two quite distinct power electronics-based 'flexible AC transmission systems' devices is presented. In particular, the damping of low frequency electromechanical oscillations is investigated aiming at improving the performance of power systems. The comparison is made using frequency domain methods under the 'individual channel analysis and design' framework. A synchronous generator feeding into a system with large inertia is used for such a purpose. Two system configurations including compensation are analysed: (a) in series in the form of a thyristor-controlled series compensator, and (b) in shunt through a static VAr compensator featuring a damping controller. Analyses are carried out to elucidate the dynamic behaviour of the synchronous generator in the presence of the power electronics-based controllers and for the case when no controller is present. Performance and robustness assessments are given particular emphasis. The crux of the matter is the comparison between the abilities of the static VAr compensator and the thyristor-controlled series compensator to eliminate the problematic switch-back characteristic intrinsic to synchronous generator operation by using the physical insight afforded by 'individual channel analysis and design'.

1. Introduction

Active power transfers may be increased and adjusted by varying the net impedance of a series-compensated line. The thyristor-controlled series compensator (TCSC), a well-developed member of the 'flexible AC transmission systems' (FACTS) device family, is the electronically-controlled counterpart of the series bank of capacitors [1,2]. Its major benefits are its ability to regulate power flows along the compensated line and to rapidly modulate the effective line impedance in response to dynamic events in the vicinity. On the other hand, the static VAr compensator (SVC), a mature member of the FACTS technology, provides dynamic reactive power support to enable an effective voltage regulation and to enhance

* Corresponding author.
E-mail addresses: Ugalde-LooC@cardiff.ac.uk (C.E. Ugalde-Loo), enrique.acha@tut.fi (E. Acha).

https://doi.org/10.1016/j.apm.2018.02.008
0307-904X/

Nomenclature

2×2, 3×3	2-input 2-output, 3-input 3-output multivariable system;
α	SVC or TCSC firing angle;
B_{SVC}	SVC total susceptance;
$C_i(s)$	i th individual channel from input $u_i(s)$ to output $y_i(s)$;
Δ	incremental change, linearised variable;
$d_i(s)$	i th external disturbance in a multivariable system;
E_{fd}	generator field voltage;
$e_i(s)$	i th error in a closed-loop multivariable system;
e_t	generator terminal voltage;
f_0	Electrical frequency;
$\gamma_i(s)$	i th multivariable structure function;
$\gamma_a(s)$	multivariable structure function of a 2×2 multivariable system;
$\Gamma_i(s)$	i th multivariable structure function (potential performance and coupling);
$\mathbf{G}_{ijk}$	transfer matrix with transfer functions associated to $C_i(s)$ in the 1st row;
$g_{ij}(s)$	ij th element of a transfer matrix;
$\mathbf{G}_{SVC}(s)$, $\mathbf{G}_{TCSC}(s)$	transfer matrix of the synchronous generator SVC/TCSC system;
H	generator inertia constant;
$h_i(s)$	i th closed-loop subsystem in a multivariable system;
I_{SVC}, I_{TCSC}	SVC output current, current flowing through the TCSC;
I_∞	current injected at the infinite bus;
j	complex operator;
k_d	damping controller stabiliser gain;
$K_D(s)$	damping controller transfer function;
$k_{ij}(s)$	ij th element of a multivariable controller;
$\mathbf{K}_{SVC}(s)$, $\mathbf{K}_{TCSC}(s)$	multivariable controller of the synchronous generator SVC/TCSC system;
$\mathbf{M}_{ik}(s)$	multiple channel with individual channels i and k;
P_g, Q_g	active, reactive power at the generator terminals;
P_m	mechanical power supplied to the generator;
$\mathbf{P}_{SVC}(s)$	post-compensator matrix of the synchronous generator SVC system;
s	Laplace operator;
σ	real part of complex conjugate roots;
τ_1, τ_2	time constants of lead/lag compensator (damping controller);
τ'_{d0}, τ'_{q0}	generator open circuit d, q-axis transient time constant;
τ''_{d0}, τ''_{q0}	generator open circuit d, q-axis sub-transient time constant;
τ_w	time constant of wash-out filter (damping controller);
$\mathbf{u}_{SVC}(s)$, $\mathbf{u}_{TCSC}(s)$	input vector of synchronous generator SVC/TCSC system;
U_{SVC}	SVC terminal voltage;
U_∞	infinite bus voltage;
ω	rotor speed;
ω_d, ω_n	damped natural frequency, natural frequency of complex conjugate roots;
X_C, X_L	capacitive, inductive reactances;
X_d, X_q	generator synchronous reactance of d, q-axis;
X'_d, X'_q	generator transient synchronous reactance of d, q-axis;
X''_d, X''_q	generator sub-transient synchronous reactance of d, q-axis;
X_t, X_{t1}, X_{t2}	tie-line reactance, tie-line reactance subjected to $X_t = X_{t1} + X_{t2}$;
X_{TCSC}	TCSC total reactance;
$y_i(s)$	i th output of a multivariable system;
$\mathbf{y}_{SVC}(s)$, $\mathbf{y}_{TCSC}(s)$	output vector of synchronous generator SVC/TCSC system;
ζ	damping ratio of complex conjugate roots.

transient stability [2]. Moreover, it has been shown that the SVC is able to damp electromechanical oscillations through an additional damping control loop [3–5].

Notwithstanding that the primary tasks of the TCSC and the SVC differ, their ability to damp low frequency electromechanical oscillations (between 0.1 and 2 Hz) to improve the power system dynamic performance by ameliorating the switch-back characteristic intrinsic to synchronous generator (SG) operation invites a comparison between these quite distinct devices. In this paper, the mathematical modelling, analysis, control system design and simulation of electrical power systems featuring these FACTS devices are addressed. A fifth-order SG feeding into a large system via a tie-line system is con-

sidered. Two configurations are studied. The first one includes a series compensator in the form of a TCSC. In the second case a shunt compensator in the form of an SVC is examined. The analysis and control system design are carried out under the frequency domain in a multivariable context by using the 'individual channel analysis and design' (ICAD) framework [6,7].

In ICAD, Bode and Nyquist plots are extensively used, together with a detailed analysis of the multivariable structure function (MSF) [8,9]. The use of ICAD to carry out dynamical studies and small-signal stability assessments allows the understanding of the dynamic interactions occurring among different power system components in a clear manner. Through this approach, physical insight is favoured over mathematical abstraction, aiming at effective evaluations of control system performance and robustness. For further information on the ICAD framework, the reader is referred to [6], where ICAD is presented, its use for multivariable control is discussed in detail, and an emphasis on robust stability is made; [7], where the structural analysis for general m-input and m-output systems is discussed, the influence of right half-plane zeros on controller design and closed-loop performance is evidenced, and the existence of fixed stabilising controllers in the presence of system uncertainty is established; [8], where the MSF characteristics for a range of 2×2 plants are studied; [9], where the MSF properties are extended to the general $m \times m$ case; and to [10], where the detailed treatment for 3×3 and 4×4 plants is examined. The framework has been successfully employed in a number of applications, ranging from submarines [11], induction motors [12,13] and wind turbines [14,15].

The damping capabilities of shunt and series FACTS devices have been studied in the literature and even comparisons been drawn. For instance, in [16] a time-domain approach is followed, with the main emphasis being on the control of reactive power to provide damping. In [17], a robust control method in the time-domain is used to design control laws for the SVC and TCSC based on the definition of energy functions. However, both devices are installed in the same test system, so it is not possible to examine the damping contribution of each component individually. Reference [18] proposes an interesting approach to evaluate the damping contribution of FACTS devices. State-space representations are formulated in terms of synchronising and damping coefficients, leading to a low-order simplified frequency domain model based on the swing equation of the SG. With such model it is possible to define performance indices key to the analysis. However, the application of these concepts is done for the TCSC only. The approach taken in this paper to address the damping capabilities of both the SVC and TCSC differs from the aforementioned methodologies since: (a) as opposed to [16,17], the FACTS devices are analysed using frequency domain tools and, as opposed to [18], the SG representation considers the electrical dynamics and is not restricted to the swing equation only; (b) contrary to [16–18], the analysis is fully multivariable, where the nature of the plant is encapsulated in transfer functions; (c) the system dynamic structure (i.e. both poles/eigenvalues and zeros) is comprehensively analysed, which is something not considered by [16,17] and is restricted to an eigenvalue analysis in [18]; and (d) the control system performance is made explicitly available with its robustness assessment, which is only carried out in [17].

Even when a great volume of research work and knowledge concerning power systems oscillations is available in the open literature, the work presented in this paper goes beyond the state of the art as a thorough comparison of the damping capabilities of the SVC and TCSC has been presented, for the first time, using a multivariable analysis and control system design framework that relies entirely on classical control tools. Preliminary results were reported in [19], but now this paper gives a detailed assessment of the dynamic responses of these devices. Owing to the elucidating properties of ICAD concerning stability and structural robustness, system performance to meet customer specifications, and the dynamical structure of multivariable systems (both for minimum and non-minimum phase systems), the knowledge gained by applying ICAD cannot be achieved with the use of eigenvalue-based analyses. As such, the mathematical approach here presented provides new analysis tools to generate knowledge in power systems research.

It should be highlighted that this paper builds on work previously published by the authors. The SG – TCSC system and SG – SVC system models adopted in this work have been previously presented in [20] and [21], respectively, where individual elements of the frequency domain models as a function of system parameters are explicitly provided. To avoid an unnecessary duplication of work, the deduction of these models is not included here and only reference to them is made in Section 2 for completeness. The individual elements of the transfer function matrices are only calculated for specific operating conditions, but these are provided as supplementary content for the interested reader. In addition, reference [4] builds on [21] by including a damping control loop to the SG – SVC system. In [4], the damping capabilities of the SVC are compared to those achieved by a power system stabiliser (PSS), which is a local device installed at the terminals of a synchronous machine. The PSS does not belong to the family of FACTS devices and is not based on power electronics components.

Although the synchronous generator – SVC system presented in [4] is used in this paper, the emphasis here is placed on how the abilities of an SVC, a shunt-connected power electronics-based device, measure against those provided by a TCSC, a power-electronics based device connected in series, to ameliorate the switch-back characteristic introduced by SGs. Given that ICAD represents an analysis and control system design framework yet to be consolidated in power systems applications, the scope has been restricted to single-machine infinite bus systems. This way, the effect that FACTS devices have in the SG dynamic operation can be clearly illustrated without obscuring the analysis if a complex power system configuration was employed instead. At the same time, such networks with a small number of elements are better placed to introduce key ICAD concepts. The framework and the concepts here presented should provide the basis for more complex power systems studies.

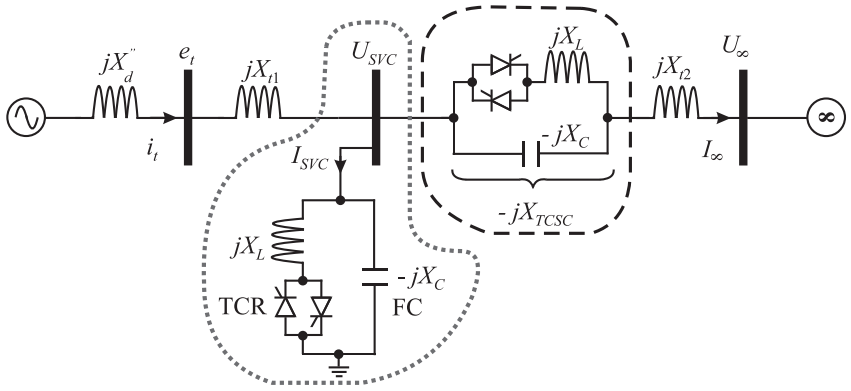

Fig. 1. One-line diagram of a SG – FACTS-upgraded system. Both TCSC and SVC configurations are shown, but a single device is used at any time.

2. SG – FACTS device-upgraded systems

The TCSC and SVC are power electronics-based devices that improve the dynamic operation of power systems. In a TCSC-upgraded system, the active power flow can be adjusted by controlling the TCSC impedance (X_{TCSC}). This is achieved by suitably changing the thyristor's firing angle (α). Conversely, an SVC is capable of drawing capacitive or inductive current from the power system. Suitable control of the equivalent reactance allows a continuous voltage regulation at the node of connection [2].

The main application of each FACTS controller is clearly different; however, both devices can be employed to damp electromechanical oscillations by acting on the problematic switch-back characteristic exhibited by SGs. Such phenomenon is caused by a resonance (lightly damped left hand plane pole -LHPP- pair) followed by an inverted resonance (lightly damped left hand plane zero -LHPZ- pair) present around 7 rad/s, which reduces the SG performance due to bandwidth limitation [22]. In the case of an SVC-upgraded system with damping capabilities, an auxiliary control loop is included [4,5].

To assess the influence that the TCSC and the SVC exert on the SG dynamic characteristic, the test systems shown in Fig. 1 are employed. The TCSC is connected in series (as enclosed by the black dashed line), whereas the SVC is connected in shunt (as enclosed by the dotted grey line). Only a single device is connected at any time for the analyses carried out in this paper.

The analyses and results presented in this paper are based on the machine representation provided in [23] (6 p.u. on a 100 MVA base). The SG model corresponds to the fifth-order dynamic model presented in [22]. A TCSC with parameters of the Kayenta installation [24] is used. The device operates in its capacitive region as it is desirable to decrease the electrical length of the transmission line in order to increase active power flows [2]. The reader is referred to the supplementary file accompanying this paper for the parameters of the SG, TCSC and SVC.

Transfer function matrix representations are required for the analysis of a SG – FACTS device-upgraded system under the framework of ICAD. If a TCSC is employed, this is given by

$$\begin{aligned} \mathbf{y}_{TCSC}(s) &= \mathbf{G}_{TCSC}(s)\mathbf{u}_{TCSC}(s), \\ \begin{bmatrix} \Delta\omega(s) \\ \Delta e_t(s) \\ \Delta I_{TCSC}(s) \end{bmatrix} &= \begin{bmatrix} g_{11}(s) & g_{12}(s) & g_{13}(s) \\ g_{21}(s) & g_{22}(s) & g_{23}(s) \\ g_{31}(s) & g_{32}(s) & g_{33}(s) \end{bmatrix} \begin{bmatrix} \Delta P_m(s) \\ \Delta E_{fd}(s) \\ \Delta\alpha(s) \end{bmatrix}, \end{aligned} \tag{1}$$

where $\mathbf{G}_{TCSC}(s)$ is the transfer function matrix of the 3×3 linearised model of the SG – TCSC system. Conversely, the transfer matrix representation of the SG – SVC system with a damping loop assumes the form

$$\mathbf{y}_{SVC}(s) = \mathbf{G}'_{SVC}(s)\mathbf{u}_{SVC}(s), \tag{2}$$

where

$$\begin{aligned} \mathbf{G}'_{SVC}(s) &= \mathbf{P}_{SVC}(s)\mathbf{G}_{SVC}(s), \\ &= \begin{bmatrix} 1 & 0 & 0 \\ 0 & 1 & 0 \\ -K_D(s) & 0 & 1 \end{bmatrix} \begin{bmatrix} g_{11}(s) & g_{12}(s) & g_{13}(s) \\ g_{21}(s) & g_{22}(s) & g_{23}(s) \\ g_{31}(s) & g_{32}(s) & g_{33}(s) \end{bmatrix} \\ &= \begin{bmatrix} g_{11}(s) & g_{12}(s) & g_{13}(s) \\ g_{21}(s) & g_{22}(s) & g_{23}(s) \\ g'_{31}(s) & g'_{32}(s) & g'_{33}(s) \end{bmatrix}. \end{aligned} \tag{3}$$

$\mathbf{G}_{SVC}(s)$ is the transfer matrix of the 3×3 linearised model of the SG – SVC system and

$$g'_{3i}(s) = g_{3i}(s) - K_D(s)g_{1i}(s), \tag{4}$$

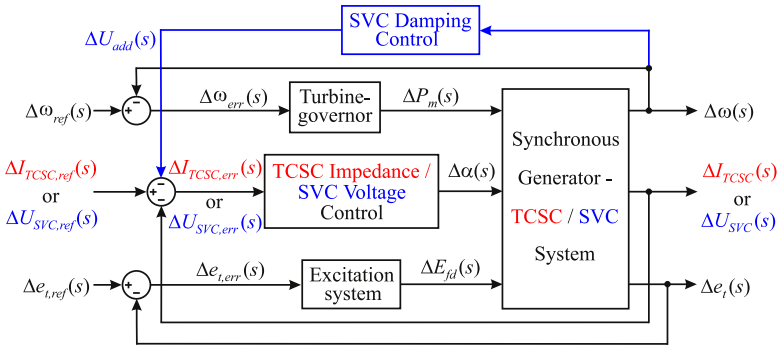

Fig. 2. Block diagram of the SG – FACTS upgraded system. If a TCSC is employed, signals are highlighted in red. Conversely, signals are highlighted in blue for an SVC with a damping loop. (For interpretation of the references to colour in this figure legend, the reader is referred to the web version of this article.)

with $i = 1, 2, 3$. In the non-diagonal post-compensator matrix $\mathbf{P}_{SVC}(s)$ in (3), the cross-coupling element $K_D(s)$ denotes the transfer function of the damping controller, conventionally given as [3]

$$K_D(s) = k_d \cdot \frac{s\tau_w}{1+s\tau_w} \cdot \frac{1+s\tau_1}{1+s\tau_2}, \tag{5}$$

where $s\tau_w/(1+s\tau_w)$ is a wash-out filter, $(1+s\tau_1)/(1+s\tau_2)$ a phase lead/lag compensator, and k_d a stabiliser gain.

The individual elements of $\mathbf{G}_{TCSC}(s)$ and $\mathbf{G}_{SVC}(s)$ can be found in [20] and [21], respectively, where they are obtained from first principles and described in detail. It should be noticed that transfer functions $g_{ij}(s)$ in (1) and (3) are dependent on system parameters and the operating condition.

Closed-loop block diagrams of the SG – TCSC system and SG – SVC system with a damping loop are shown in Fig. 2. For the case of the SG – SVC system, the "communicated" SG speed $\Delta\omega(s)$ is used as an auxiliary signal. By including this feedback loop the signal for SVC voltage control is $K_D(s)\Delta\omega(s) + \Delta U_{SVC}(s)$. The damping loop transforms a diagonal system into non-diagonal (a diagonal term plus a post-compensator) [4].

3. Multivariable analysis

Transfer matrix representations are essential for an analysis under the ICAD framework [9]. In ICAD, the dynamical structure of systems (1) and (2) is determined by individual channels resulting from pairing each input to each output by means of diagonal controllers [7]. For both cases, the pairing is given as

$$\mathbf{K}(s) = \begin{bmatrix} k_{11}(s) & 0 & 0 \\ 0 & k_{22}(s) & 0 \\ 0 & 0 & k_{33}(s) \end{bmatrix} \Rightarrow \begin{cases} C_1(s): & \Delta P_m \rightarrow \Delta\omega \\ C_2(s): & \Delta E_{fd} \rightarrow \Delta e_t \\ C_3(s): & \Delta\alpha \rightarrow \Delta U_{SVC}/\Delta I_{TCSC} \end{cases}. \tag{6}$$

The diagonal control structure in (6) agrees with conventional control strategies. Notice that individual channels $C_1(s)$ and $C_2(s)$ correspond to the input-output pairing associated to the SG [25], whereas $C_3(s)$ is associated to the SVC voltage or TCSC impedance control loop.

Fig. 3 shows the individual channel representation of the systems featuring FACTS devices. As it can be noticed, the multivariable system can be re-formulated as three SISO channels, where each channel includes a feedback loop and its controller. Each controller can be designed to comply with the specifications associated to each channel. Every channel is subject to a disturbance $d_i(s)$ – representing the effects of other channel references. Therefore, the behaviour of an individual channel will not be only affected by its controller but also by the other individual channels. The individual channel representation of Fig. 3 is fully equivalent to the original systems of Fig. 2 [6,7]. In general, the ith individual channel $C_i(s)$ in Fig. 3 has the open-loop SISO transmittance

$$C_i(s) = k_{ii}g_{ii}(1-\gamma_i), \tag{7}$$

where

$$\gamma_i(s) = -\left|\overline{\mathbf{G}}_i\right|/g_{ii}\left|\overline{\mathbf{G}}^i\right|, \tag{8}$$

subjected to disturbances

$$d_i(s) = -\left|\mathbf{R}_i\right|/g_{ii}\left|\overline{\mathbf{G}}^i\right|, \tag{9}$$

with $i = 1, 2, 3$. The multivariable character of the plant is quantified in the frequency domain by the MSFs $\gamma_i(s)$ [7–9]. In particular, for the 3×3 systems (1) and (3), the construction of matrices $\mathbf{R}_i$, $\overline{\mathbf{G}}^i$ and $\overline{\mathbf{G}}_i$ in (8)–(9) is obtained from the

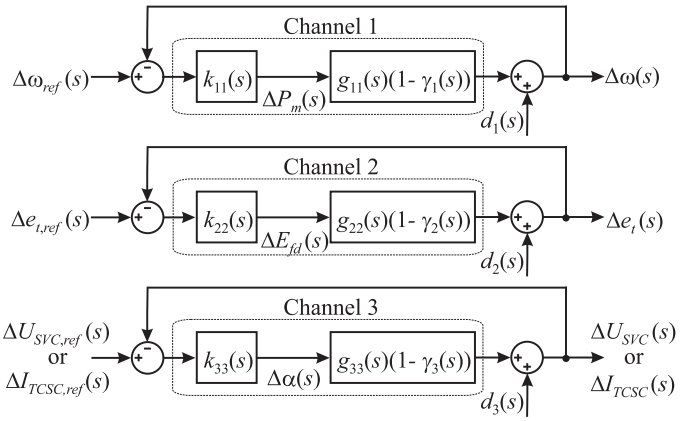

Fig. 3. Individual channel representation of the systems.

auxiliary transfer matrix

$$\overline{\mathbf{G}}(s)=\begin{bmatrix} g_{11}/h_1 & g_{12} & g_{13} \\ g_{21} & g_{22}/h_2 & g_{23} \\ g_{31} & g_{32} & g_{33}/h_3 \end{bmatrix}, \tag{10}$$

where the transfer functions $h_i(s)$ are defined as

$$h_i(s)=k_{ii}g_{ii}(1+k_{ii}g_{ii})^{-1}, \tag{11}$$

and describe the impact of controller k_{ii} on the other control loops. $\overline{\mathbf{G}}^i$ in (8) is obtained from $\overline{\mathbf{G}}$ in (10) by eliminating the ith row and ith column. Similarly, $\overline{\mathbf{G}}_i$ is obtained by setting diagonal element g_{ii}/h_i of $\overline{\mathbf{G}}$ to zero. $\mathbf{R}_i$ is defined as the matrix obtained by replacing the ith column of $\overline{\mathbf{G}}$ by the vector of channel references $\mathbf{r}$ and setting r_i to zero [7]. For example, for individual channel $C_1(s)$, MSF $\gamma_1(s)$ is expressed as

$$\begin{aligned}\gamma_1(s) &= -\left|\overline{\mathbf{G}}_1\right|/g_{11}\left|\overline{\mathbf{G}}^1\right| \\ &= -\begin{vmatrix} 0 & g_{12} & g_{13} \\ g_{21} & g_{22}/h_2 & g_{23} \\ g_{31} & g_{32} & g_{33}/h_3 \end{vmatrix} \Bigg/ \left(g_{11}\begin{vmatrix} g_{22}/h_2 & g_{23} \\ g_{32} & g_{33}/h_3 \end{vmatrix}\right).\end{aligned} \tag{12}$$

An assessment of coupling between channels is a pre-condition for an effective control system design and can be determined with auxiliary MSFs $\Gamma_i(s)$ [9]. These functions are indicators of the potential performance of feedback control. A small MSF magnitude indicates low interaction between channels. $\Gamma_i(s)$ are defined as [7]:

$$\Gamma_i(s)=-\left|\mathbf{G}_i^{12\ldots(i-1)}\right|/g_{ii}\left|\mathbf{G}^{12\ldots(i-1)i}\right|, \tag{13}$$

where $\mathbf{G}^{12\ldots(i-1)i}$ is obtained from the plant matrix $\mathbf{G}(s)$ by eliminating the 1st row and column and so on up to the ith row and column. $\mathbf{G}_i^{12\ldots(i-1)}$ is defined as the matrix obtained by setting diagonal term g_{ii} of $\mathbf{G}(s)$ to zero before eliminating the rows and columns as in the definition of $\mathbf{G}^{12\ldots(i-1)i}$. For a 3×3 system,

$$\begin{aligned}\Gamma_1(s) &= -\left|\mathbf{G}_1\right|/g_{11}\left|\mathbf{G}^1\right| = -\begin{vmatrix} 0 & g_{12} & g_{13} \\ g_{21} & g_{22} & g_{23} \\ g_{31} & g_{32} & g_{33} \end{vmatrix} \Bigg/ \left(g_{11}\begin{vmatrix} g_{22} & g_{23} \\ g_{32} & g_{33} \end{vmatrix}\right) \\ &= \frac{-[-g_{12}(g_{21}g_{33}-g_{23}g_{31})+g_{13}(g_{21}g_{33}-g_{22}g_{31})]}{g_{11}(g_{22}g_{33}-g_{23}g_{32})},\end{aligned} \tag{14}$$

$$\begin{aligned}\Gamma_2(s) &= -\left|\mathbf{G}_2^1\right|/g_{22}\left|\mathbf{G}^{12}\right| = -\begin{vmatrix} 0 & g_{23} \\ g_{32} & g_{33} \end{vmatrix} \Big/ \left(g_{22}\ |g_{33}\ |\right) \\ &= g_{23}g_{32}/g_{22}g_{33}.\end{aligned} \tag{15}$$

In order to assess the MSFs it is convenient to introduce the following notation. Transfer matrices in (1) and (3) will be called from now on $\mathbf{G}_{123}$, where the subscripts indicate that the transfer functions associated to the output of $C_1(s)$ occupy the first row, those of $C_2(s)$ the second row, and those of $C_3(s)$ the third row. When analysing $\mathbf{G}_{123}$, $\Gamma_1(s)$ quantifies the coupling between individual channel $C_1(s)$ and multiple channel $\mathbf{M}_{23}(s)$ [formed by individual channels $C_2(s)$ and $C_3(s)$], and $\Gamma_2(s)$ among individual channels $C_2(s)$ and $C_3(s)$. For a system $\mathbf{G}_{321}$, the first and third rows and columns are swapped

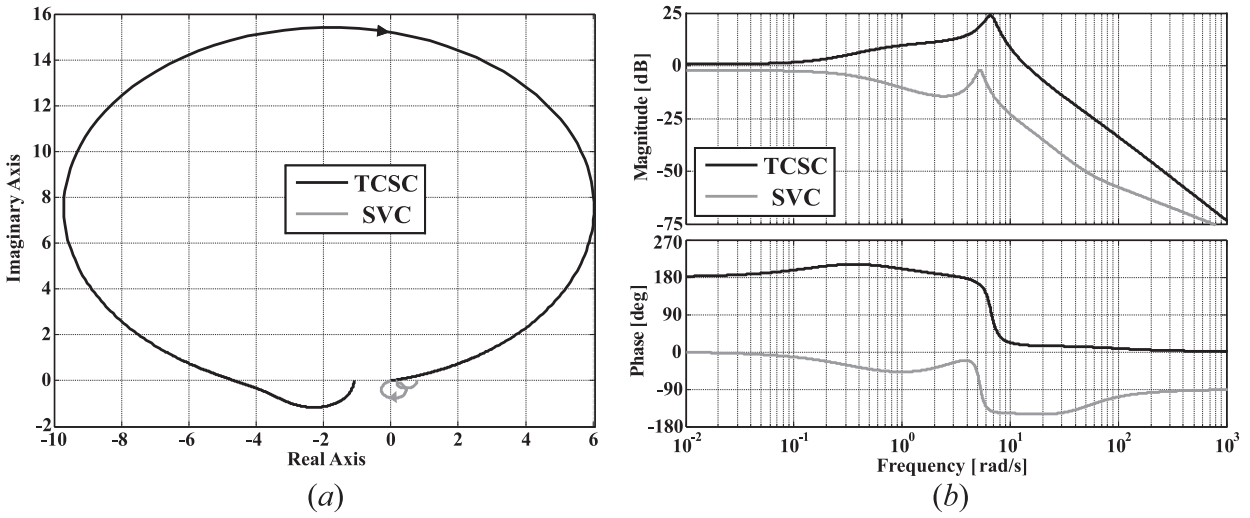

Fig. 4. $\Gamma_1(s)$ assessment (transfer matrix $\mathbf{G}_{123}$): (a) Nyquist plot; (b) Bode plot.

in relation to the original transfer matrix $\mathbf{G}_{123}$. In this case, $\Gamma_1(s)$ provides a measure of coupling between $C_3(s)$ and $\mathbf{M}_{12}(s)$ and $\Gamma_2(s)$ quantifies the coupling between $C_1(s)$ and $C_2(s)$.

It should be noticed that (14) and (15) have been defined for $\mathbf{G}_{123}$ and will not hold, for instance, for transfer matrix $\mathbf{G}_{321}$; thus, $\Gamma_1(s)$ and $\Gamma_2(s)$ should be constructed accordingly for each new transfer matrix. Moreover, although six possible combinations of transfer matrices are possible for a 3×3 system, the MSFs of some of them offer identical information (*e.g.*, $\mathbf{G}_{123}$ and $\mathbf{G}_{132}$, $\mathbf{G}_{213}$ and $\mathbf{G}_{231}$, and $\mathbf{G}_{312}$ and $\mathbf{G}_{321}$) [7].

3.1. Comparison between FACTS devices

The TCSC performance is compared with that of an SVC featuring a damping control loop. A weak transmission system comprising a SG connected to an infinite bus via a tie-line reactance ($X_t = 0.7$ p.u.) is considered. Both devices are connected at the mid-point of the line. The operating conditions and transfer matrices $\mathbf{G}_{TCSC}(s)$ and $\mathbf{G}_{SVC}(s)$ in (1) and (3) evaluated in those conditions are provided in the supplementary file accompanying this paper. The following SVC damping controller has been considered:

$$K_D(s) = \frac{3.6s(s+3.333)}{(s+0.4)(s+0.1)}, \tag{16}$$

where $k_d = 30$, $\tau_w = 10$ s, $\tau_1 = 0.3$ s and $\tau_2 = 2.5$ s. $K_D(s)$ was designed to modify the SVC's transfer functions $g_{31}(s)$, $g_{32}(s)$ and $g_{33}(s)$ to, respectively, $(g_{31} - K_D g_{11})$, $(g_{32}(s) - K_D g_{12})$ and $(g_{33}(s) - K_D g_{13})$. By doing so, the switch-back characteristic particularly exhibited by $g_{32}(s)$ and $g_{33}(s)$ is dominated by the inverted notch effect introduced by $K_D(s)$.

A numerical evaluation of MSFs $\Gamma_i(s)$ (for relevant transfer matrices $\mathbf{G}_{123}$, $\mathbf{G}_{213}$ and $\mathbf{G}_{312}$) corresponding to $\mathbf{G}_{TCSC}(s)$ and $\mathbf{G}_{SVC}(s)$ shows that they are minimum-phase and stable. The interested reader can prove this through suitable use of (14) and (15) and the transfer functions provided in the supplementary file accompanying the paper. Moreover, their Nyquist plots start to the left of the point (1, 0). Such features simplify the control system design. Figs. 4–9 show the MSFs of the TCSC system (1) and of transfer matrix (3) of the SVC system when damping controller (16) is used. The analysis is described next.

3.1.1. TCSC analysis

After assessment of Figs. 4–9 it is observed that:

- With reference to transfer matrix $\mathbf{G}_{123}$: Multiple channel $\mathbf{M}_{23}(s)$ is highly coupled with individual channel $C_1(s)$ at frequencies around the switch-back characteristic (above 0 dB for frequencies below 11 rad/s) even at high series compensation values, as shown in the plots of MSF $\Gamma_1(s)$ in Fig. 4. $C_2(s)$ and $C_3(s)$ within $\mathbf{M}_{23}(s)$ are also coupled (see Fig. 5).
- $\mathbf{G}_{213}$: $\mathbf{M}_{13}(s)$ is coupled with $C_2(s)$ due to the high level of series compensation, as evidenced by Fig. 6. $C_1(s)$ and $C_3(s)$ within $\mathbf{M}_{13}(s)$ are highly coupled (above 0 dB for frequencies below 11 rad/s), as shown by Fig. 7.
- $\mathbf{G}_{312}$: $\mathbf{M}_{12}(s)$ is highly coupled with $C_3(s)$ at low frequencies, as shown in Fig. 8. However, $C_1(s)$ and $C_2(s)$ within $\mathbf{M}_{12}(s)$ are weakly coupled due to the effect of series compensation (see Fig. 9).

From the aforementioned remarks it can be stated that the inclusion of the TCSC produces a highly coupled system. Coupling is high particularly at low frequencies over the range of interest of [1, 10] rad/s where the switch-back character-

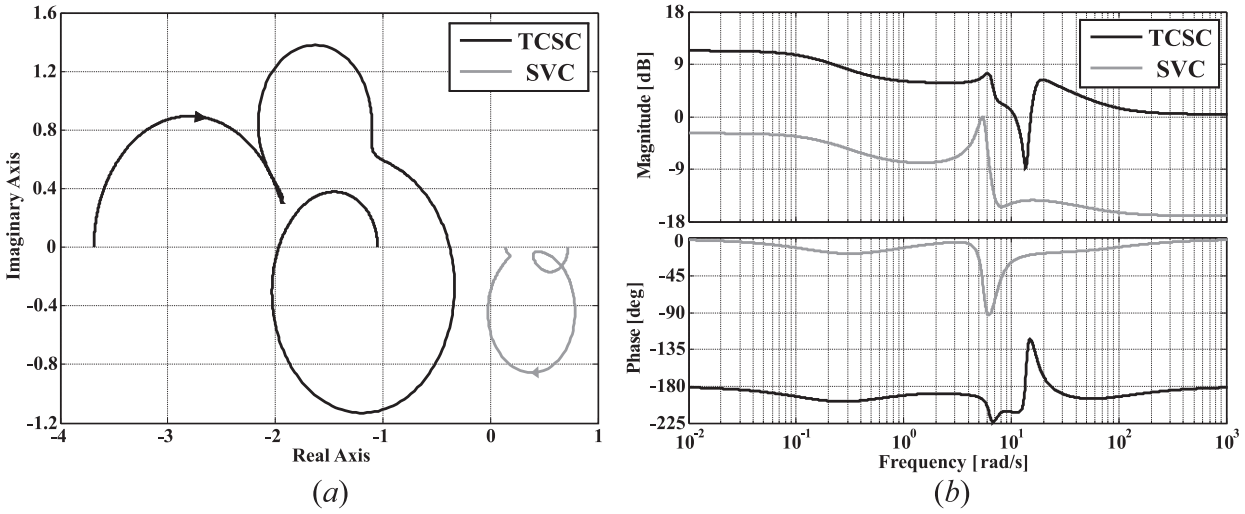

Fig. 5. $\Gamma_2(s)$ assessment (transfer matrix $\mathbf{G}_{123}$): (a) Nyquist plot; (b) Bode plot.

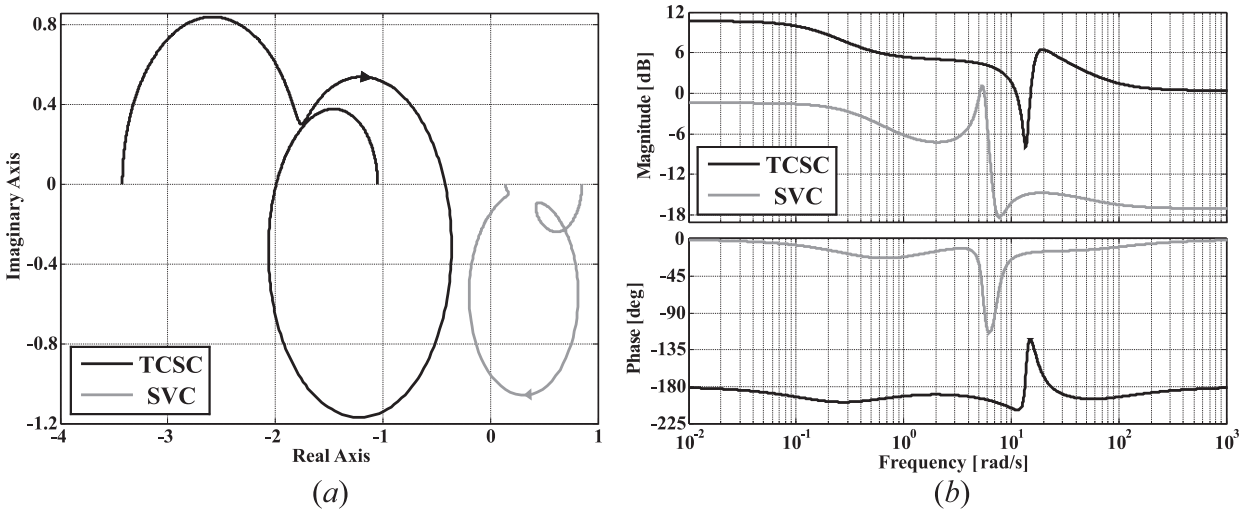

Fig. 6. $\Gamma_1(s)$ assessment (transfer matrix $\mathbf{G}_{213}$): (a) Nyquist plot; (b) Bode plot.

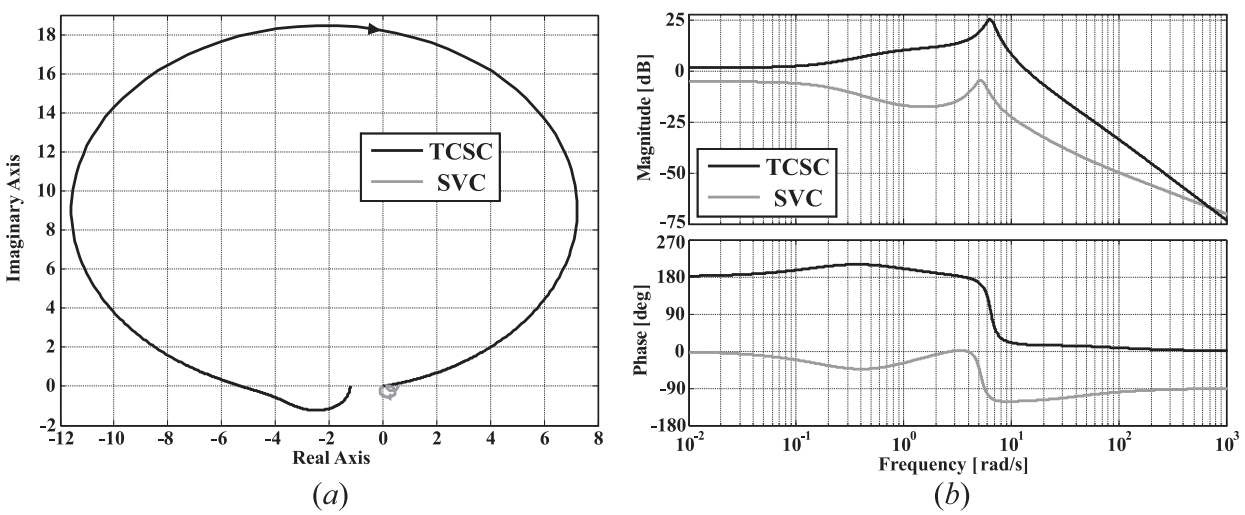

Fig. 7. $\Gamma_2(s)$ assessment (transfer matrix $\mathbf{G}_{213}$): (a) Nyquist plot; (b) Bode plot.

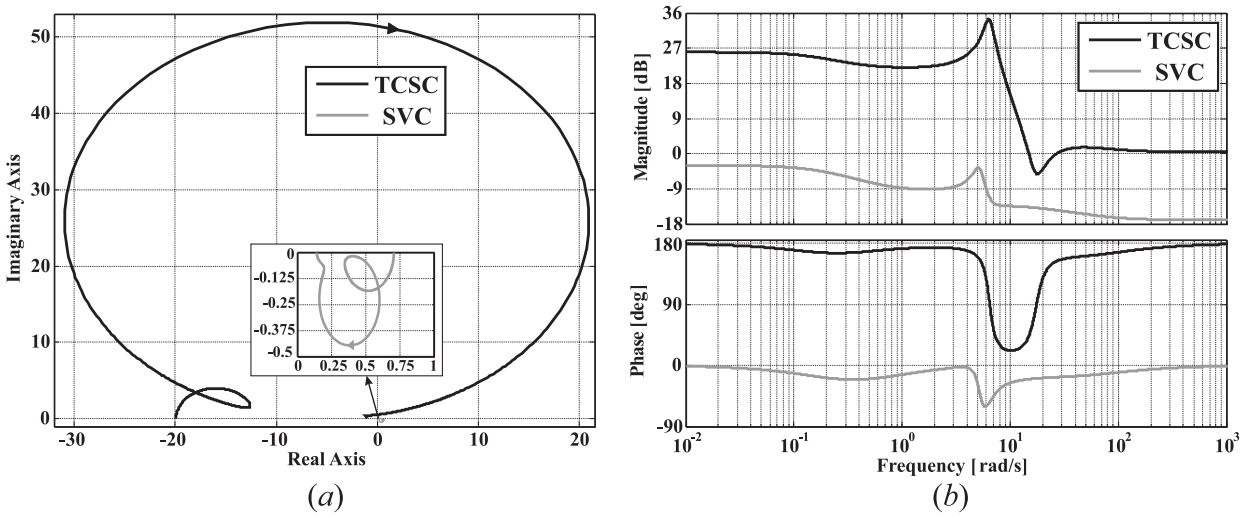

Fig. 8. $\Gamma_1(s)$ assessment (transfer matrix $\mathbf{G}_{312}$): (a) Nyquist plot; (b) Bode plot.

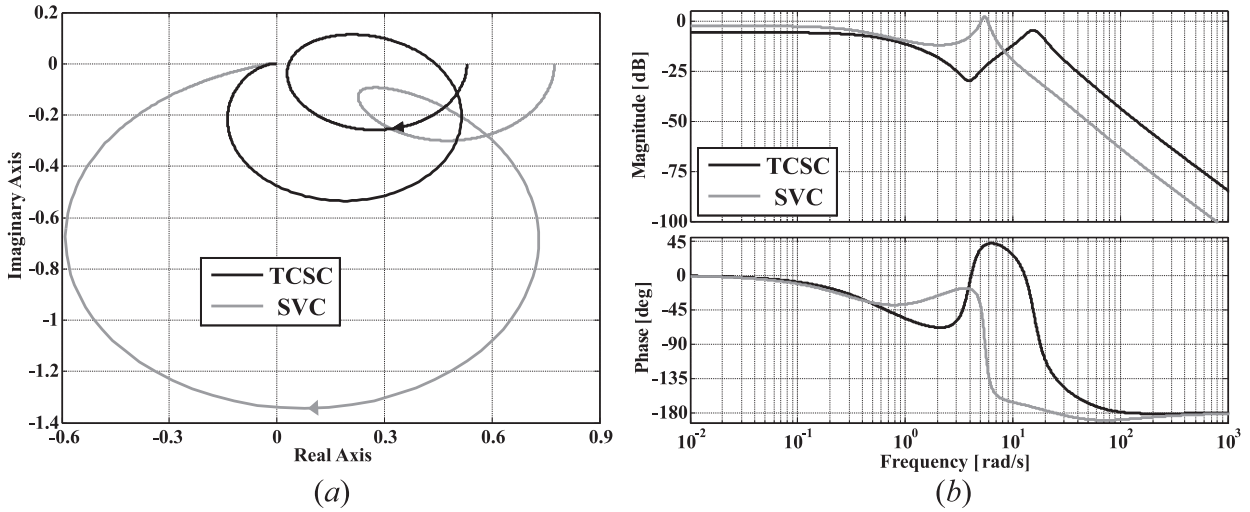

Fig. 9. $\Gamma_2(s)$ assessment (transfer matrix $\mathbf{G}_{312}$): (a) Nyquist plot; (b) Bode plot.

istic occurs. Moreover, the TCSC impedance control loop, represented by $C_3(s)$, significantly couples with the speed channel of the SG; *i.e.,* $C_1(s)$.

3.1.2. SVC analysis

The following conclusions can be made:

- $\mathbf{G}_{123}$: $\mathbf{M}_{23}(s)$ couples with $C_1(s)$ around the switch-back characteristic (but below 0 dB), as shown by $\Gamma_1(s)$ in Fig. 4. As seen from $\Gamma_2(s)$ in Fig. 5, the coupling between $C_2(s)$ and $C_3(s)$, although it increases around the problematic frequencies, is affected by the inverse notch characteristic provided by the damping loop.
- $\mathbf{G}_{213}$: $\mathbf{M}_{13}(s)$ is slightly coupled with $C_2(s)$ (near 0 dB at frequencies around the switch-back characteristic), as shown by $\Gamma_1(s)$ in Fig. 6. $C_1(s)$ and $C_3(s)$ couple around the switch-back characteristic, as evidenced by $\Gamma_2(s)$ in Fig. 7. However, coupling is below 0 dB.
- $\mathbf{G}_{312}$: $\mathbf{M}_{12}(s)$ couples with $C_3(s)$ around the switch-back characteristic, as shown by $\Gamma_1(s)$ in Fig. 8; however, coupling is below 0 dB. From $\Gamma_2(s)$ in Fig. 9, it is noticed that the coupling between $C_1(s)$ and $C_2(s)$ is weak, but increases around the switch-back characteristic.

It can be concluded that the SVC and the SG constitute a slightly coupled multivariable system particularly at frequencies over the range of interest of [1, 10] rad/s. The SVC voltage control loop, represented by $C_3(s)$, couples with the terminal voltage channel of the SG. The SG inner coupling (between $C_1(s)$ and $C_2(s)$) is not reduced by the use of the damping loop. However, an immediate benefit brought about by the damping loop lies on the elimination of the switch-back characteristic.

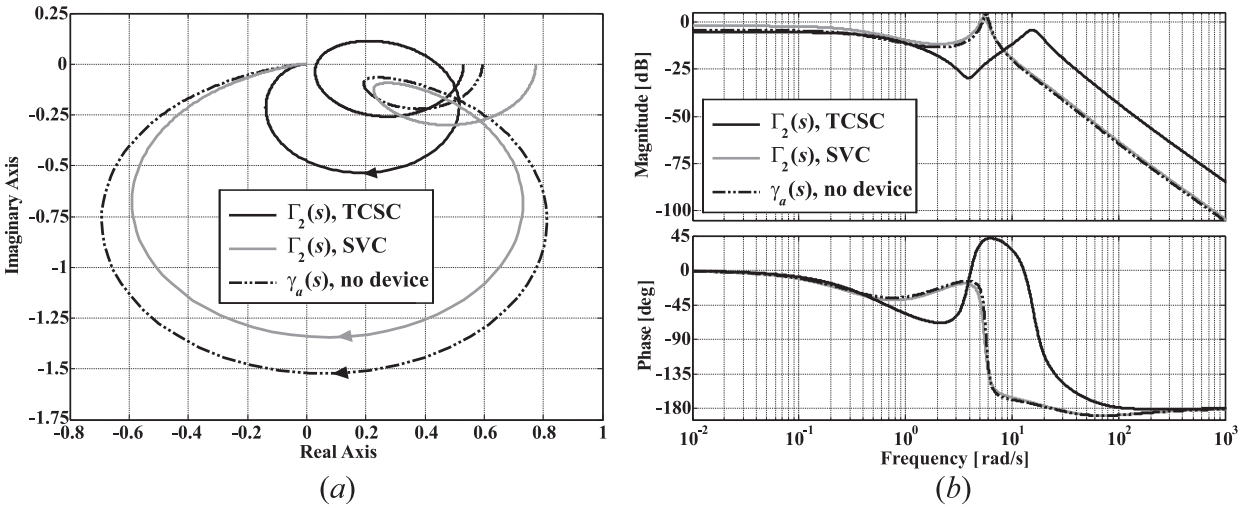

Fig. 10. Assessment of MSFs with and without compensation: (a) Nyquist plot; (b) Bode plot.

Such an effect is introduced directly by elements associated to the SVC voltage channel $C_3(s)$. Due to the existent coupling between $C_2(s)$ and $C_3(s)$ damping will be indirectly provided to $C_2(s)$ and the switch-back characteristic can be substantially reduced [4,19].

3.2. Analysis with no compensation

The SG dynamics under the influence of the TCSC or the SVC are represented by $\mathbf{M}_{12}(s)$. The Nyquist and Bode plots of MSF $\Gamma_2(s)$ -for transfer matrix $\mathbf{G}_{312}$- quantify the internal coupling of the SG under the influence of the FACTS device [4,20,21]. Conversely, the uncompensated 2×2 system $\mathbf{G}_{SG}(s)$ is described by

$$\begin{aligned} \mathbf{y}_{SG}(s) &= \mathbf{G}_{SG}(s)\mathbf{u}_{SG}(s), \\ \begin{bmatrix} \Delta\omega(s) \\ \Delta e_t(s) \end{bmatrix} &= \begin{bmatrix} g_{11}(s) & g_{12}(s) \\ g_{21}(s) & g_{22}(s) \end{bmatrix} \begin{bmatrix} \Delta P_m(s) \\ \Delta E_{fd}(s) \end{bmatrix}, \end{aligned} \tag{17}$$

The construction of $\mathbf{G}_{SG}(s)$ is provided in detail in [22]. The individual elements of $\mathbf{G}_{SG}(s)$ can be found in the supplementary file accompanying this paper. Considering the traditional channel pairing as in (6), the MSF for system (17) reduces to

$$\gamma_a(s) = g_{12}g_{21}/g_{11}g_{22}. \tag{18}$$

MSFs $\Gamma_2(s)$ (using $\mathbf{G}_{312}$) for the systems featuring shunt or series compensation are compared with the MSF $\gamma_a(s)$ for the system with no FACTS device -$\mathbf{G}_{SG}(s)$- in Fig. 10. It can be noticed that the coupling in the SG with no auxiliary devices, given by MSF $\gamma_a(s)$, changes little around the switch-back characteristic frequencies with respect to that of the system with SVC. The SVC damping loop does not alter the internal coupling since its direct impact is not on the speed or terminal voltage channels, as shown by its MSF $\Gamma_2(s)$. $\Gamma_2(s)$ corresponding to the TCSC shows a reduced coupling due to a decreasing electrical distance of the transmission line. The peak moves on to higher frequencies but it is still pronounced.

It is well-known that the robustness of transmission systems decreases when the electrical distance of the lines is increased. Moreover, coupling within the SG is low under a lagging power factor operation and relatively short tie-lines; however, it increases with electrical distance. It has also been shown that the larger the amount of reactive power flow in the tie-line reactance the higher the coupling between channels [22]. These results are important since they may dictate a control design strategy shared by the two cases here studied. For instance, $\mathbf{M}_{12}(s)$ corresponding to the SG can be designed independently of the FACTS device associated to $C_3(s)$.

3.3. Clarifying observations on the use of ICAD for robust control design

ICAD is not a method for achieving optimal control in a physical system for all sets of operating conditions and will not provide a set of rules to design optimal controllers. Given that the control design process depends on the dynamic characteristics of the plant to be controlled, a design strategy may guarantee an excellent performance for a specific system, but it may not be nearly as effective for another one.

The multivariable analysis afforded by ICAD presented in this section enables the design of highly robust controllers as long as the frequency domain information provided by the MSFs is interpreted correctly. A detailed analysis has been performed for SVC and TCSC-upgraded systems and when no compensator is used. By elucidating the restrictions exhibited

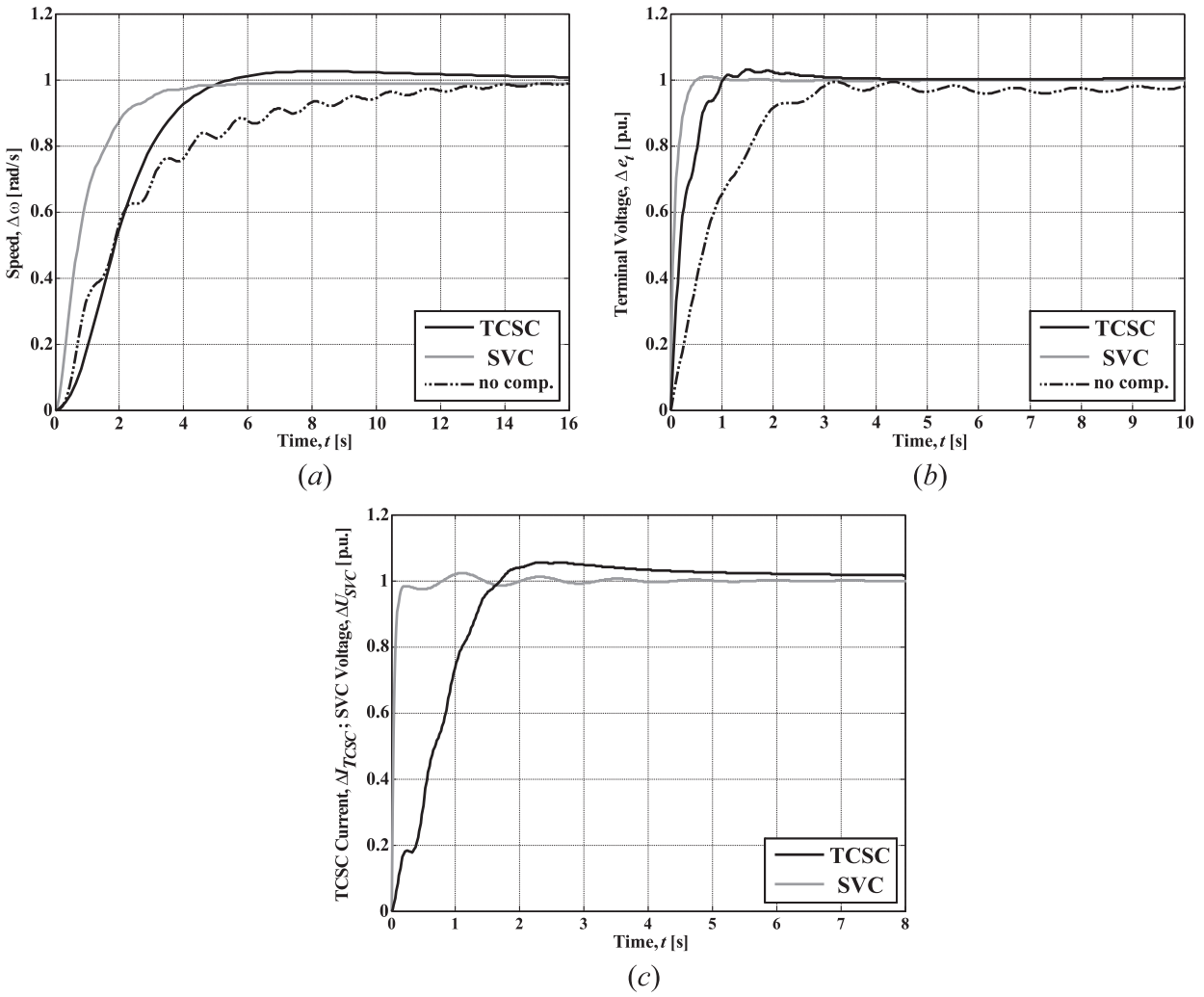

Fig. 11. System performance. Step response: (a) Channel 1 [$T_{c1}(s)$]; (b) Channel 2 [$T_{c2}(s)$]; (c) Channel 3 [$T_{c3}(s)$].

by the uncontrolled plants, highly robust controllers can be designed for each system so that the best performance is achieved for a given operating condition. This will be examined in Section 4.

It should be highlighted that a loss of effectiveness and performance could be expected as the operating conditions depart from those under which the control system design is carried out; however, this issue may be significantly limited if the controller exhibits high robustness measures. If stability and structural robustness are achieved (within the restrictions set by the plant itself), the control system is expected to operate well under parametric variations, to reject disturbances, to attenuate high frequency noise and to perform well upon deviations from the nominal operating conditions.

4. Control system design comparison

System performance can be compared using suitably designed controllers. For the SG – TCSC system,

$$\mathbf{K}_{TCSC} = \mathrm{diag}\left[\frac{5.8(s^2+6.1s+165.5)}{s^2(s+5)(s+6)},\quad \frac{76(s+7)(s+1)(s+0.2)}{s(s+3.5)(s+3)},\quad \frac{-0.07(s+0.2)}{s(s+7)(s+0.7)}\right] \tag{19}$$

is used. For the SG – SVC system,

$$\mathbf{K}_{SVC} = \mathrm{diag}\left[\frac{63(s+3.5)(s^2+s+30)}{s^2(s+6)(s+5)},\quad \frac{107.5(s+0.43)}{s},\quad \frac{400}{s}\right] \tag{20}$$

and (16) are used. When no compensation is included,

$$\mathbf{K}_{SG} = \mathrm{diag}\left[\frac{2.9(s^2+6.1s+165.5)}{s^2(s+5)},\ \frac{7(s+0.43)}{s}\right] \tag{21}$$

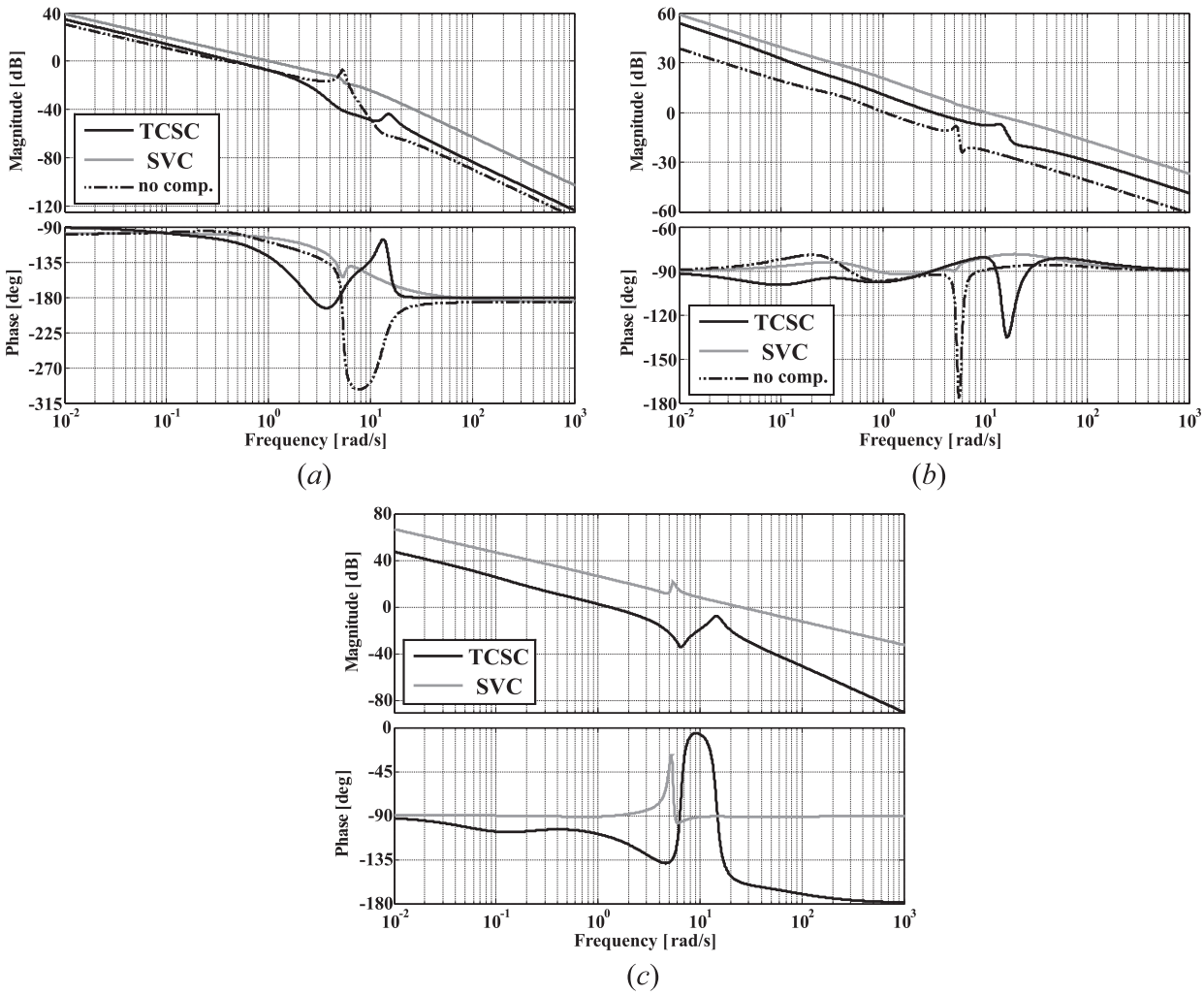

Fig. 12. System performance and stability robustness assessment. Bode diagrams: (a) $C_1(s)$; (b) $C_2(s)$; (c) $C_3(s)$.

is used. The design of these controllers has been performed in the frequency domain using Bode shaping techniques. Notice that $k_{11}(s)$ and $k_{22}(s)$ in (19)–(21) have a similar structure, with differences arising in gains and lead terms. For all cases, $k_{11}(s)$ has two integral actions to cancel out the derivative term present in $g_{11}(s)$ (see the supplementary file accompanying the paper) and to ensure a zero steady-state error. The inclusion of zero/pole pairs (as lead compensators) ensures high phase margins. With regards to $k_{22}(s)$, the basic control structure in all cases is a proportional-integral controller (PI); i.e., an integral action, a proportional gain, and a suitably placed zero. This basic configuration ensures a zero steady-state error and is sufficient to achieve a good performance for the SG – SVC system and for the SG without any compensation. However, it is necessary to include a couple of lead compensators to $k_{22}(s)$ for the SG – TCSC system to maximise the stability margins.

The structure of $k_{33}(s)$ is different for each FACTS-upgraded configuration. Although $g_{33}(s)$ for both systems has a similar structure (refer to the supplementary file accompanying the paper), it should be noticed that the sign of the transfer function when a TCSC is used is negative. Therefore, $k_{33}(s)$ should consider this 180 degrees phase shift by including a negative gain. The overall structure is basically a PI controller that achieves a zero steady-state error and two suitably placed poles to ensure an adequate roll-off beyond the cut-off frequency. Conversely, the structure of $k_{33}(s)$ for the SVC-upgraded system considers just an integral action which ensures a zero steady-state error and a proportional gain to achieve the desired the bandwidth. The control system performance and robustness indicators for each system are presented in Figs. 11–14. Key information is summarised in Table 1.

Fig. 11 shows the step responses. The performances of $C_1(s)$ (speed) and $C_2(s)$ (terminal voltage) are adequate with either FACTS device (Fig. 11(a)–(b)). The step response of $C_3(s)$ (Fig. 11(c)) shows that for the SVC system oscillations occur due to the presence of complex poles. Slower step responses in the TCSC upgraded system are due to the chosen bandwidths. Without series or shunt compensation, the responses are slightly oscillatory even with a bandwidth limitation.

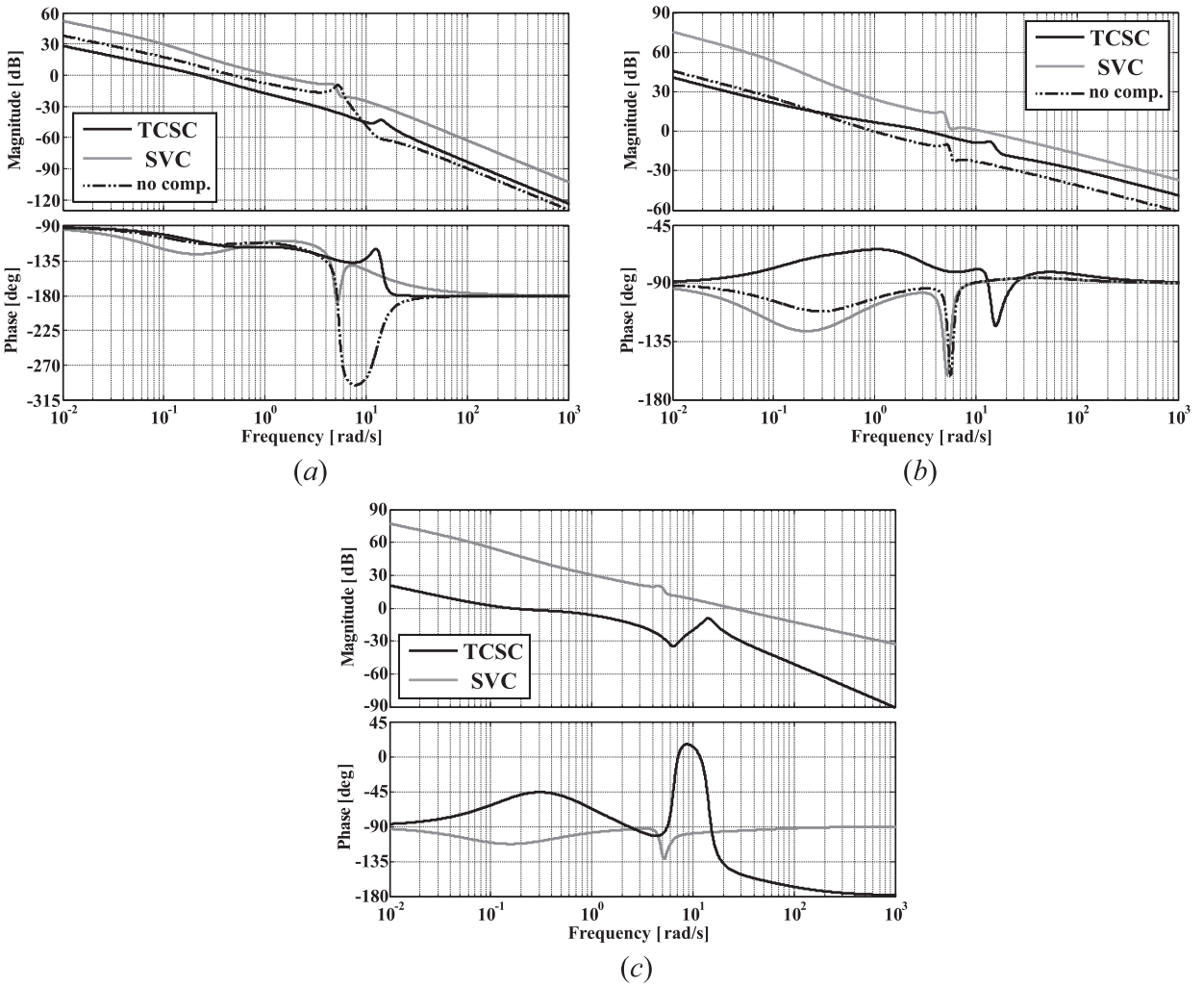

Fig. 13. Stability robustness assessment. Bode diagrams: (a) $k_{11}g_{11}(s)$; (b) $k_{22}g_{22}(s)$; (c) $k_{33}g_{33}(s)$.

Table 1
Structural and stability robustness of the channels and control systems.

Device	Measure	$C_1(s)$	$k_{11}g_{11}(s)$	$\gamma_1(s)$	$C_2(s)$	$k_{22}g_{22}(s)$	$\gamma_2(s)$	$C_3(s)$	$k_{33}g_{33}(s)$	$\gamma_3(s)$
	Bandwidth [rad/s]	0.625	0.29	–	4.5	4.7	–	1.67	0.477	–
TCSC	Gain margin [dB]	21.2	60.9	10.2	∞	∞	47.3	∞	∞	∞
	Phase margin [deg]	70.6	70.5	54.9	90	105	113.6	68.6	127	102.7
	Bandwidth [rad/s]	1.46	1.68	–	15.6	17.4	–	34	34.2	–
SVC	Gain margin [dB]	∞	11	2.2	∞	∞	1.4	∞	∞	3.0
	Phase margin [deg]	85.3	70.8	∞	99.2	91.2	38.6	88.8	84	24.4
	Bandwidth [rad/s]	0.596	0.633	–	1.41	1.35	–	–	–	–
No Device	Gain margin [dB]	8.18	10.1	4.82	∞	∞	4.82	–	–	–
	Phase margin [deg]	92.7	67.3	∞	83.3	78	∞	–	–	–

Fig. 12 shows the Bode plots of the individual channels. Together with Table 1 it is observed that both control systems with FACTS devices offer adequate roll-off and stability margins (*i.e.*, gain and phase margins over 6 dB and 40 deg [25]) for the speed channel, although the SVC with the damping loop offers the best performance. It is clear from Fig. 12(b) that the SVC damping loop eliminates the switch-back characteristic in the terminal voltage channel, and as a result, an arbitrary high bandwidth can be achieved (notice the significantly higher gain of $k_{22}(s)$ in (20) for the SVC system compared to that for the SG without compensation in (21)). For the TCSC system, the amount of series compensation has been adjusted to 80%. As it can be seen the switch-back characteristic is not completely eliminated even when such a high compensation is used. Thus, the bandwidth has to be reduced producing a slower $C_2(s)$. From Fig. 12(c) it can be seen that for the SVC the inverted notch

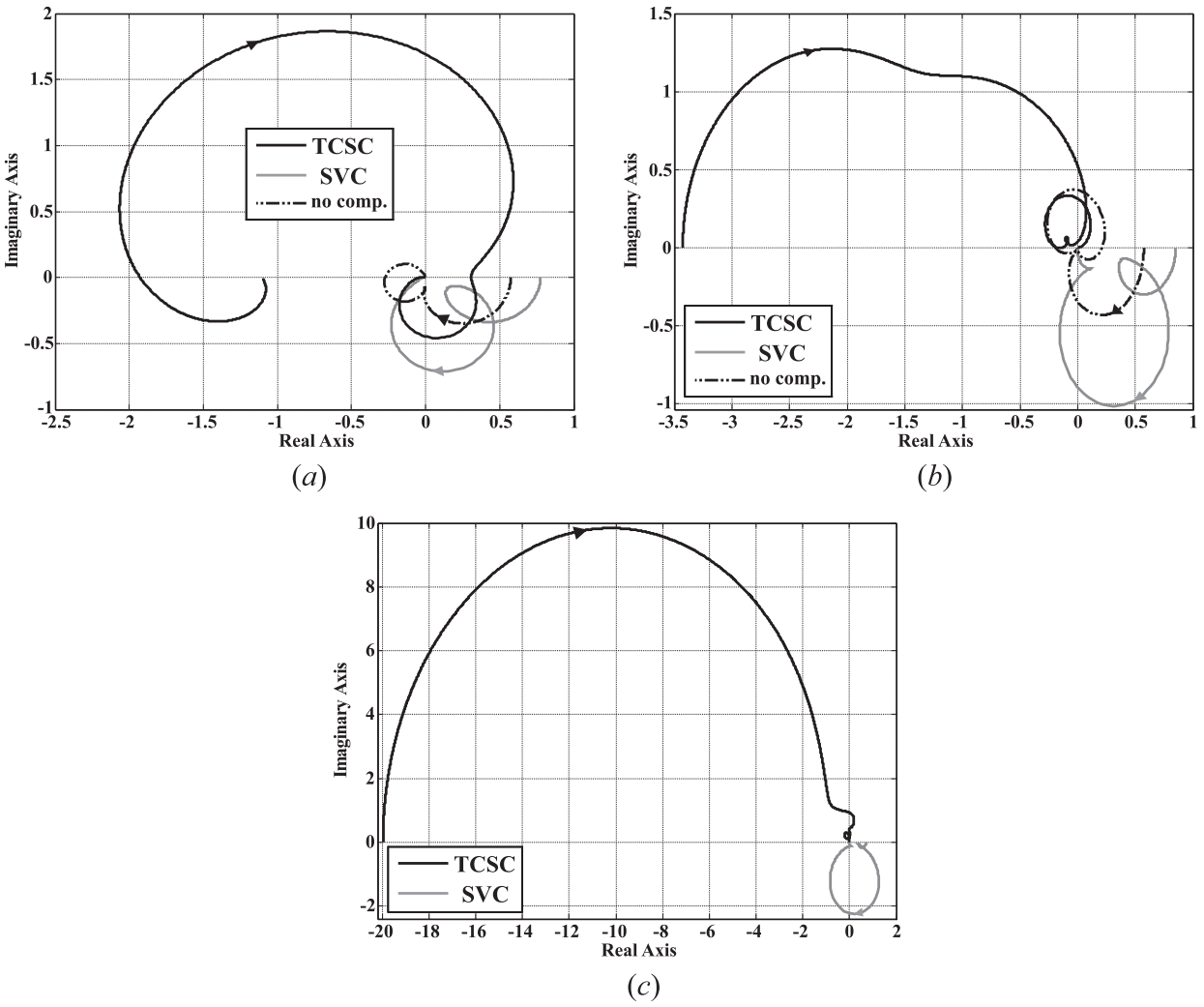

Fig. 14. Structural robustness assessment. Nyquist diagrams: (a) $\gamma_1(s)$; (b) $\gamma_2(s)$; (c) $\gamma_3(s)$.

characteristic is dominant around the switch-back characteristic in $C_3(s)$; thus, a high bandwidth can be achieved. When the TCSC is in use, the combination of resonant complex conjugate zero/pole pairs suggests a reduced bandwidth.

When no compensation is used, the bandwidth has to be limited in $C_1(s)$ to avoid instability, as shown in Fig. 12(a). The gain margin is small although still above 6 dB. From Fig. 12(b), the switch-back characteristic featured in $C_2(s)$ is quite pronounced when no series or shunt devices are included. Thus, the only option for this system configuration is to restrict the bandwidth, as it can be noticed in Table 1, which is reflected on the slower step responses in Figs. 11(a) and 11(b). This has been achieved by reducing the proportional gain of $k_{11}(s)$ and $k_{22}(s)$ in (21).

The structural robustness of the control systems is assessed in Figs. 13 and 14. Fig. 13 shows the Bode diagrams of the individual channel open loop subsystems $h_i(s)$ [i.e., $k_{ii}g_{ii}(s)$]. It can be seen that the SVC fails to eliminate fully the switch-back characteristic in $h_2(s)$ (see Fig. 13(b)) since the damping controller has a direct influence only in $g_{33}(s)$. Obviously, the problem occurs as well on the uncompensated system. Clearly the TCSC reduces, but does not eliminate the switch-back characteristic. As shown in Fig. 14, all MSFs $\gamma_i(s)$ start to the left to (1, 0) and the roll-off behaviour is adequate. Due to this condition the small gain margins of the MSFs and their proximities to (1, 0) are irrelevant; *i.e.*, the electrical distance of the tie-line is considerably long and its reduction would only increase these margins.

A good control system performance with satisfactory robustness margins is obtained with either a TCSC or a SVC with a damping loop. However, the TCSC effectiveness can be constrained to the amount of reactive power produced by the SG. Moreover, it is evident from the TCSC characteristic that the higher the amount of compensation required the closer the firing angle is to the resonant point –with parametric variations capable of leading to series resonance [20]. Extreme care should be exercised when operating in this area. The use of the SVC with a damping loop allows the switch-back characteristic elimination –thus enabling a higher disturbance rejection and bandwidth in the terminal voltage channel.

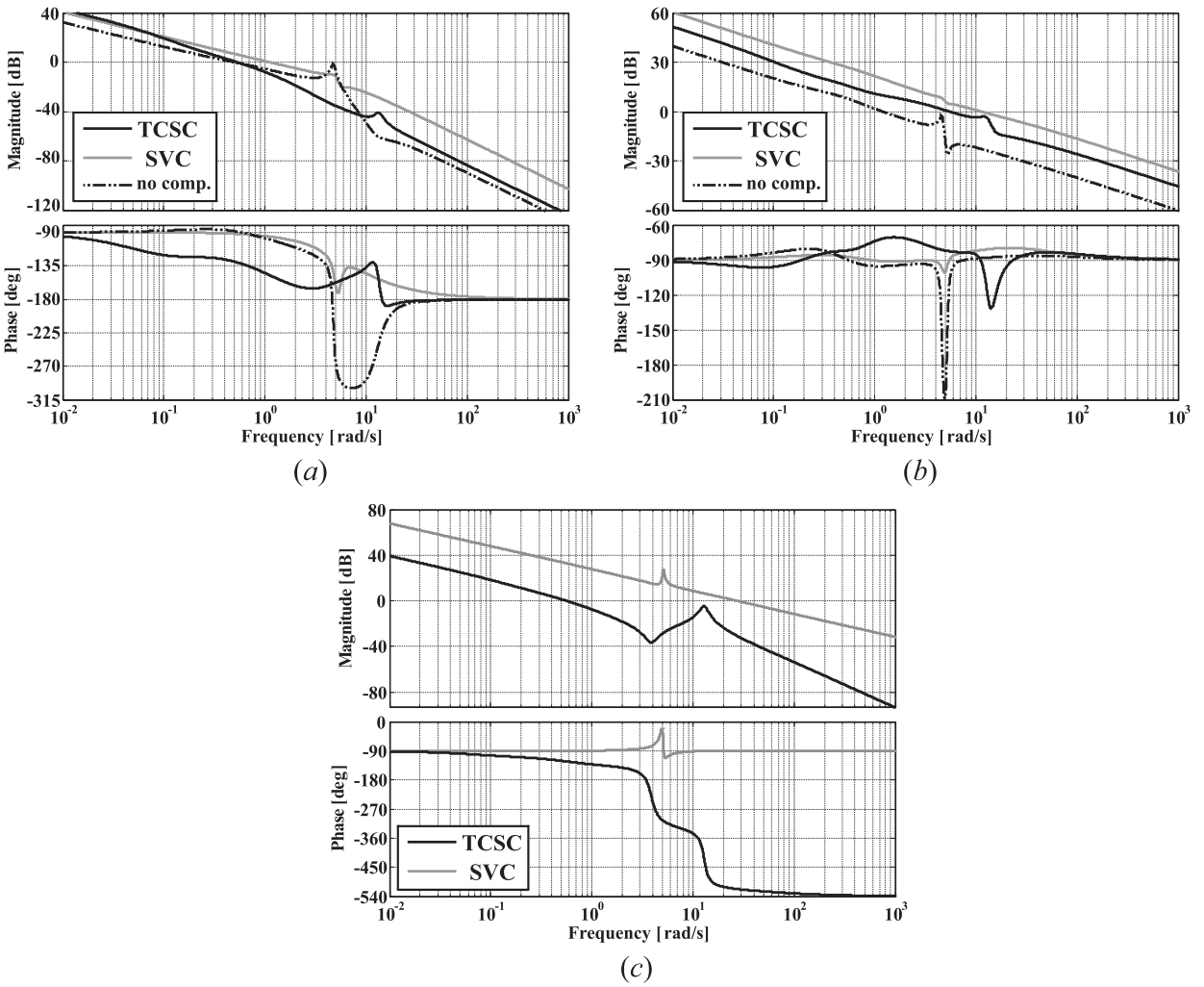

Fig. 15. Performance and stability robustness assessment (long transmission line). Bode diagrams: (a) $C_1(s)$; (b) $C_2(s)$; (c) $C_3(s)$.

If no compensation is used the performance has to be restricted. As the switch-back characteristic is quite prominent only bandwidth limitation remains as the only valid option to operate the system while still preserving adequate stability margins.

Note: The results reported in this section show that the shunt compensator outperforms the series compensator in terms of damping power systems oscillations in a generic power system. Although the SVC and the TCSC are significantly different FACTS devices, the comparison is quite fair as a similar design objective has been adopted: the reduction of the problematic switch-back characteristic exhibited by SGs.

Although it could be argued that the control designs for the SVC and the TCSC may not be optimal, both control systems exhibit very high stability margins with measures that surpass by far the minimum requirements recommended in power systems for a good performance [25] – the reader is kindly refereed to the gain and phase margins of the individual channels in Table 1. The multivariable controllers yield a very satisfactory performance for the set of operating conditions for which they have been designed. Moreover, the structure of the individual elements of the control matrices is simple: only integral actions, PI controllers, and PI controllers cascaded with lead compensators have been employed. Admittedly, system performance could be improved even more, but the marginal benefits for doing this would be at the expense of using more complex control structures than those in (19) and (20). Very complex controllers are not suitable for practical power systems.

5. A closer look at the TCSC performance

The TCSC impedance control channel can feature right half plane zeros (RHPZ) under certain operating conditions. It is well known that RHPZs have adverse effects in the control system performance and sensitivity [26]. To avoid such a scenario, the percentage of series compensation has to be maximised.

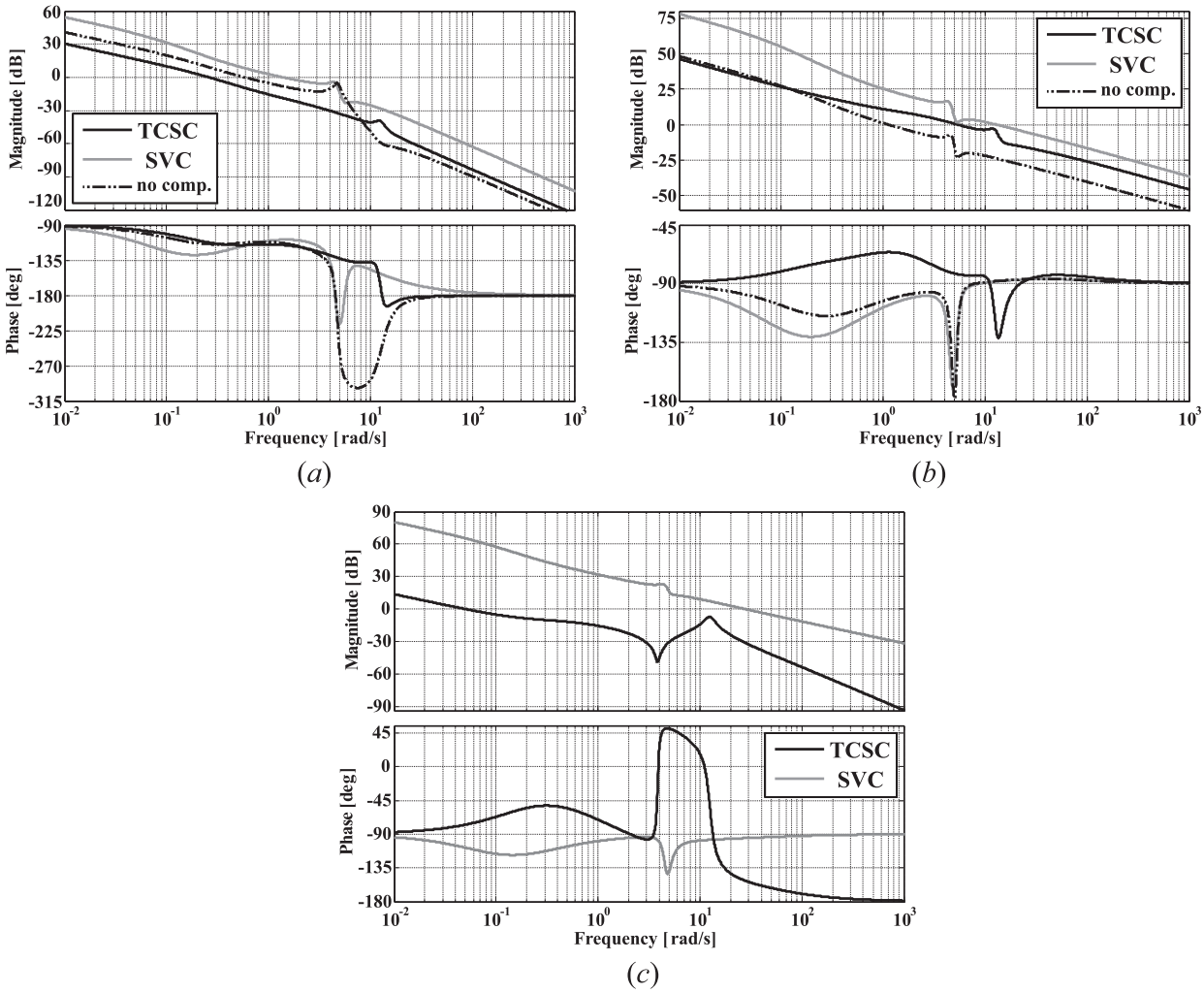

Fig. 16. Stability robustness assessment (long transmission line). Bode diagrams: (a) $k_{11}g_{11}(s)$; (b) $k_{22}g_{22}(s)$; (c) $k_{33}g_{33}(s)$.

Table 2
Structural and stability robustness of the channels and control systems. Long transmission line.

Device	Measure	$C_1(s)$	$k_{11}g_{11}(s)$	$\gamma_1(s)$	$C_2(s)$	$k_{22}g_{22}(s)$	$\gamma_2(s)$	$C_3(s)$	$k_{33}g_{33}(s)$	$\gamma_3(s)$
	Bandwidth [rad/s]	0.69	0.338	–	8.49	8.11	–	0.715	0.07	–
TCSC	Gain margin [dB]	43.4	40.6	9.6	∞	∞	34.2	32.6	∞	12.4
	Phase margin [deg]	49.8	67.6	93	97.5	97.1	∞	57.2	103	106
	Bandwidth [rad/s]	1.59	2.03	–	17.2	19.1	–	38.3	38.6	–
SVC	Gain margin [dB]	∞	4.82	1.95	∞	∞	1.21	∞	∞	2.33
	Phase margin [deg]	84.5	71.1	55.13	98.5	91.6	41.53	88.9	84.7	23.77
	Bandwidth [rad/s]	0.745	0.79	–	1.65	0.83	–	–	–	–
No Device	Gain margin [dB]	2.64	6.03	4.14	4.25	∞	4.14	–	–	–
	Phase margin [deg]	91.8	67.1	∞	84.7	77.8	∞	–	–	–

In order to have a closer look at the effect of RHPZs the TCSC performance is assessed while considering a longer electrical distance ($X_t = 0.8$ p.u.) and a value of 70% series compensation. The operating condition is shown in the supplementary file accompanying the paper. System performance is assessed using the same controllers as in Section 4. The control system performance and robustness indicators are presented in Figs. 15–17. Key information is summarised in Tables 2 and 3. The responses associated to the system without compensation reflect in a poorer performance than in Section 4 due to the increase in the transmission line length, but the same conclusions apply. Thus, no further discussion is warranted.

Fig. 15 shows the Bode plots of the individual channels. Notice that the SVC still offers a good performance and successfully eliminates the switch-back characteristic in spite of increasing the transmission line length. Although the control design

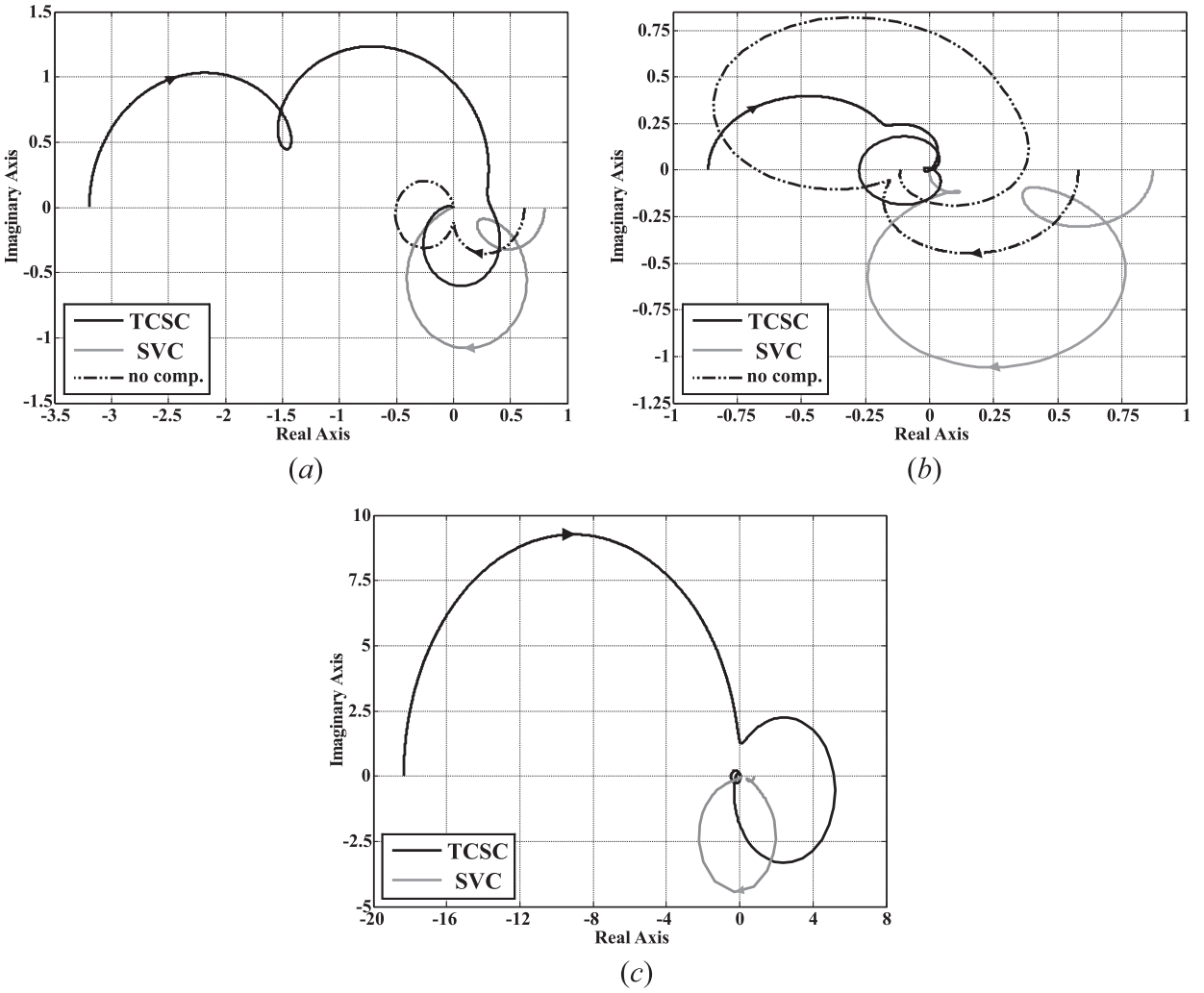

Fig. 17. Structural robustness assessment (long transmission line). Nyquist diagrams: (a) $\gamma_1(s)$; (b) $\gamma_2(s)$; (c) $\gamma_3(s)$.

Table 3
$C_3(s)$ non-minimum phase assessment.

Non-minimum phase term	RHPZs	Damped natural freq. ω_d [rad/s]	Natural freq. ω_n [rad/s]	Damping ratio ζ	Bandwidth [rad/s]
$(s^2 - 0.8327s + 15.4)$	$0.41635 \pm j3.8687$	3.868	3.891	−0.107	0.715

for the TCSC system offers adequate stability margins for the three individual channels (see Table 2), $C_3(s)$ has an non-minimum phase complex conjugate zero pair of the form $(s^2 - 2\zeta\omega_n s + \omega_n^2)$ with roots $Z_{1,2} = \sigma \pm j\omega_d = \zeta\omega_n \pm j\omega_n\sqrt{1-\zeta^2}$, where ω_n is the natural frequency, ζ is the damping ratio and ω_d is the damped natural frequency. The RHPZs (shown in Table 3) in the TCSC impedance channel are lightly damped with a small damping ratio. This can be noted in Fig. 15(c): the magnitude plot shows a significant resonance at ω_n of the zero pair ($\approx$4 rad/s), while 180 deg are quickly lost in the phase plot. The presence of RHPZs poses a major inconvenience for the control system design: the bandwidth of $C_3(s)$ should be kept below ω_n of the non-minimum phase zero pair; otherwise, instability might arise. Moreover, it is not possible to arbitrarily reduce sensitivity to uncertainty [26]. While in Section 4 the bandwidth was decreased to avoid an oscillatory behaviour due to resonant complex zero/pole pairs, in this case the reduction is mandatory to avoid instability.

The structural robustness of the control system is assessed in Figs. 16 and 17. The stability margins of $k_{11}g_{11}(s)$ in both the SVC and TCSC systems decrease due to the effect of a longer transmission line. It can be seen in Fig. 17(c) that MSF $\gamma_3(s)$ of the TCSC system encircles the point (1, 0) in clockwise direction producing a non-minimum phase $C_3(s)$ with the adverse implications previously described.

6. Conclusion

A detailed comparison of the dynamical impact of two distinct FACTS controllers on a SG is presented – they are the TCSC and the SVC. Multivariable control system analyses and designs of the SG as affected by these FACTS configurations, using the framework of ICAD, have been carried out. Key aspects of the SVC and TCSC operation have been revealed by applying ICAD, which may not have been possible to clarify, at least not as emphatically, by other forms of analysis methods (e.g., eigenanalysis, block diagrams, synchronising/damping coefficients). Simulation results are in agreement with system behaviour observed in practice.

The TCSC and SVC abilities to damp low frequency electromechanical oscillations to improve power system performance by reducing the SG switch-back characteristic have been investigated. It has been shown that although the main task of the SVC is to enhance voltage regulation, an auxiliary damping control loop yields quite a satisfactory performance. The SVC damping control loop can be represented as a post-compensator of the speed output. Its success stems from the exploitation of the SG dynamics in order to overcome the switch-back characteristic, and consequently, a higher bandwidth can be achieved. The primary task of the TCSC is to reduce the electrical length of the transmission line to maximise active power transfers. However, the TCSC has also the capacity to damp power oscillations by attenuating the switch-back characteristic and shifting it to higher frequencies.

ICAD reveals that the TCSC brings fragility to the system as it introduces cross-coupling. It may also introduce RHPZs in one channel, thus, limiting the performance. Although for very high compensation levels the system remains minimum phase, the practical significance of this is debatable since it is achieved at close proximity to the resonant point of the TCSC characteristic – a forbidden area of operation, with the potential to cause permanent equipment damage and injury to personnel. In addition, a substantial increase of series compensation comes together with other issues, such as the increment in reactive power supplied by the SG, high fault currents, possible difficulties in power flow control and resonance implications.

Supplementary material

Supplementary material associated with this article can be found, in the online version, at 10.1016/j.apm.2018.02.008.

References

[1] IEEE, FACTS Overview, IEEE Press, USA, 1995.
[2] E. Acha, C.R. Fuerte-Esquivel, H. Ambriz-Perez, C. Angeles-Camacho, FACTS Modelling and Simulation in Power Networks, IEEE Press, USA, 2004.
[3] H.F. Wang, Interaction analysis and co-ordination of SVC voltage and damping control, in: Proceedings of 2000 IEEE International Conference on Electric Utility Deregulation and Restructuring and Power Technologies 2, London, UK, 4–7 April, 2000, pp. 361–365.
[4] C.E. Ugalde-Loo, E. Acha, E. Licéaga-Castro, Fundamental analysis of the electromechanical oscillation damping control loop of the static VAr compensator using individual channel analysis and design, IEEE Trans. Power Deliv. 25 (2010) 3053–3069.
[5] A.E. Hammad, Analysis of power system stability enhancement by static VAr compensators, IEEE Trans. Power Syst. 1 (1986) 222–227.
[6] J. O'Reilly, W.E. Leithead, Multivariable control by 'individual channel design', Int. J. Control 54 (1991) 1–46.
[7] W.E. Leithead, J. O'Reilly, M-input m-output feedback control by individual channel design part 1. structural issues, Int. J. Control 56 (1992) 1347–1397.
[8] E. Liceaga-Castro, J. Liceaga-Castro, C.E. Ugalde-Loo, Beyond the existence of diagonal controllers: from the relative gain array to the multivariable structure function, in: Proceedings of the 44th IEEE Conference on Decision and Control, and the European Control Conference 2005, Sevilla, Spain, 12–15 December, 2005, pp. 7150–7156.
[9] L.A. Amézquita-Brooks, C.E. Ugalde-Loo, E. Licéaga-Castro, J. Licéaga-Castro, The multivariable structure function as an extension of the RGA matrix: relationship and advantages, Cybern. Phys. 2 (2013) 53–62.
[10] C.E. Ugalde-Loo, Dynamical modelling of power systems with power electronic controllers using individual channel analysis and design. (Ph.D. dissertation), The University of Glasgow, 2009.
[11] E. Licéaga-Castro, J. Licéaga-Castro, C.E. Ugalde-Loo, E.M. Navarro-López, Efficient multivariable submarine depth-control system design, Ocean Eng. 35 (2008) 1747–1758.
[12] L.A. Amézquita-Brooks, J. Licéaga-Castro, E. Licéaga-Castro, C.E. Ugalde-Loo, Induction motor control: Multivariable analysis and effective decentralized control of stator currents for high-performance applications, IEEE Trans. Ind. Electron. 62 (2015a) 6818–6832.
[13] L.A. Amézquita-Brooks, E. Licéaga-Castro, J. Licéaga-Castro, C.E. Ugalde-Loo, Flux-torque cross-coupling analysis of FOC schemes: novel perturbation rejection characteristics, ISA Trans. 58 (2015b) 446–461.
[14] J.L. Domínguez-García, C.E. Ugalde-Loo, O. Gomis-Bellmunt, F.D. Bianchi, Input-output signal selection for damping of power system oscillations using wind power plants, Int. J. Electric. Power Energy Syst. 58 (2014) 75–84.
[15] C.E. Ugalde-Loo, L.A. Amézquita-Brooks, E. Licéaga-Castro, J. Licéaga-Castro, Analysis and efficient control design for generator-side converters of PMSG-based wind and tidal stream turbines, in: Proceedings of the 18th Power Systems. Computation Conference, Wroclaw, Poland, 18–22 August, 2014, pp. 1–7.
[16] L. Angquist, B. Lundin, J. Samuelsson, Power oscillation damping using controlled reactive power compensation-a comparison between series and shunt approaches, IEEE Trans. Power Syst. 8 (1993) 687–700.
[17] M. Noroozian, M. Ghandhari, G. Andersson, J. Gronquist, I. Hiskens, A robust control strategy for shunt and series reactive compensators to damp electromechanical oscillations, IEEE Trans. Power Deliv. 16 (2001) 812–817.
[18] E.V. Larsen, J.J. Sanchez-Gasca, J.H. Chow, Concepts for design of FACTS controllers to damp power swings, IEEE Trans. Power Syst. 10 (1995) 948–956.
[19] C.E. Ugalde-Loo, E. Acha, E. Licéaga-Castro, Comparison between series and shunt FACTS controllers using individual channel analysis and design, in: Proceedings of the 2010 45th Universities Power Engineering Conference, Cardiff, Wales, UK, 31 August - 3 September, 2010, pp. 1–7.
[20] C.E. Ugalde-Loo, E. Acha, E. Licéaga-Castro, L. Vanfretti, Individual channel analysis of the thyristor-controlled series compensator performance, Int. J. Emerg. Electr. Power Syst. 11 (2010) 1–46.
[21] C.E. Ugalde-Loo, E. Acha, E. Licéaga-Castro, J.U. Licéaga-Castro, Fundamental analysis of the static VAr compensator performance using individual channel analysis and design, Int. J. Emerg. Electr. Power Syst. 9 (2008) 1–35.
[22] C.E. Ugalde-Loo, L. Vanfretti, E. Licéaga-Castro, E. Acha, Synchronous generators modeling and control using the framework of individual channel analysis and design: Part 1, Int. J. Emerg. Electr. Power Syst. 8 (2007) 1–28.

[23] T.J. Hammons, D.J. Winning, Comparisons of synchronous-machine models in the study of the transient behaviour of electrical power systems, Proc. Inst. Electr. Eng. 118 (1971) 1442–1458.
[24] N. Christl, R. Heddin, K. Sadek, P. Lutzelberger, P.E. Krause, S.M. McKenna, A.H. Montoya, D. Torgerson, Advanced series compensation (ASC) with thyristor controlled impedance, in: Proceedings of CIGRÉ, 14/37/38-05, Paris, France, 1992.
[25] P. Kundur, Power Systems Stability and Control, McGraw-Hill, USA, 1994.
[26] J.S. Freudenberg, D.P. Looze, Right half plane poles and zeros and design tradeoffs in feedback systems, IEEE Trans. Autom. Control 30 (1985) 555–565.